Journal of ELECTRONIC MATERIALS, Vol. 46, No. 5, 2017
DOI: 10.1007/s11664-016-5144-7

Micro-structure and Room-Temperature Thermoelectric Properties of Bi-Doped Antimony Zinc Thin Films Fabricated by Co-sputtering Method

MENG WEI,[1] PING FAN,[1,4] ZHUANG-HAO ZHENG,[1,2,3,5] JING-TING LUO,[1,2] GUANG-XING LIANG,[1] AI-HUA ZHONG,[1] and MEI-MEI YIN[1]

1.—College of Physics and Energy, Institute of Thin Film Physics and Applications, Shenzhen University, Shenzhen 518060, China. 2.—Shenzhen Key Laboratory of Sensor Technology, Shenzhen 518060, China. 3.—Laboratory of Glasses and Ceramics, Institute of Chemical Science UMR CNRS 6226, University of Rennes 1, Rennes 35042, France. 4.—e-mail: fanping308@126.com. 5.—e-mail: zhengzh1986@126.com

In this report, Bi-doped antimony zinc thin films were prepared on BK7 glass substrates by using direct magnetron co-sputtering technique. Bi was doped at the halfway point of deposition, and the doping contents were 2 at.%, 4 at.%, and 6 at.%, respectively. We present the micro-structural and room-temperature thermoelectric properties of Bi-doped Zn-Sb thin films in this paper. The maximum value of the Seebeck coefficient was found to be 300 μV/K with a Bi content of 6 at.%. This is one of the highest values of the Seebeck coefficient for Zn-Sb thin films deposited by direct magnetron co-sputtering. Carrier concentration is obtained from Hall effect measurements, which provided insights into the transport mechanisms that affected electrical conductivity and Seebeck coefficient. It is significant to doping Bi, which enhances the power factor to an optimal value of 0. 26 mW/mK^2 and the optimal ZT value to 0.086 with the Bi content of 4 at.% at room-temperature.

Key words: Thermoelectric thin film, Bi-doped antimony zinc, co-sputtering, Bi content, room-temperature

INTRODUCTION

Because of the increasing energy demand in the world, non-traditional energy sources have become more and more important.[1] Thermoelectric materials can convert thermal energy directly to electric energy.[2] They are clean and reliable new energy materials with a wide area of applications such as electric power generation, thermal waste heat recovery, various electronic cooling devices, and solar cells.[3,4] Thermoelectricity can be a great addition to improve energy conversion efficiency.[5]

The thermoelectric property depends on the material property through the dimensionless figure of merit ZT, where T is the working temperature and Z is defined as the ratio $\sigma S^2/\kappa$ with σ is the electrical conductivity, S is the Seebeck coefficient and κ is the thermal conductivity. Power factor (PF) is defined as $S^2\sigma$. The material with higher PF and lower thermal conductivity is desired for higher ZT, $ZT = PFT/\kappa = S^2\sigma T/\kappa$.[6,7]

Compared with bulk materials, thin film materials offer a great potential to enhance the thermoelectric property of the materials. Thin films enhance the density of states near the Fermi energy, which can increase the Seebeck coefficient and decrease the thermal conductivity through increased boundary scattering.[8,9] The thermal conductivity of thin films is also highly dependent on the substrate which can be utilized to further increase the performance.[10]

In the Zn-Sb binary system, ZnSb is already understood as a thermoelectric material, and its properties were investigated 40–50 years ago.[11] ZnSb has a large

Meng Wei and Zhuang-Hao Zheng have equally contributed to this work.
(Received May 27, 2016; accepted November 12, 2016; published online November 29, 2016)

Seebeck coefficient with a reasonably high figure of merit.[12] Among them, metal doping has been widely researched to optimize its thermoelectric performance. For instance, dopants such as Pb, Bi, Mg, Cu, Co, Sn, In, Cd, Al, Ga, Nb, Hg, and Ag have been investigated so far. The results have shown that by doping with these elements, the thermoelectric properties can be slightly improved.[13–15]

In this paper, ZnSb thermoelectric thin film was prepared by co-deposition of Zn and Sb. Bi doping is used at the halfway point with different concentrations to optimize the thermoelectric property of the ZnSb based thin films.

EXPERIMENTAL PROCEDURES

A JGP-450B double chamber magnetron sputtering ultrahigh vacuum system was used, and we fabricated zinc antimony thermoelectric thin films on BK7 substrate under Ar atmosphere by co-sputtering. BK7 substrate is a glass substrate produced by Schott glass factory in Germany. It is a type of substrate used for coating. In order to remove the inherent oxides and contaminants on the surfaces of the target, a 5-min pre-sputtering process was necessary. The substrates were erased cleanly by air-laid paper after using ultrasonic cleaning for 15 min in acetone, alcohol, and deionized water, respectively. Before depositing the thin film, the substrate was covered by a metal baffle, and a pre-sputtering was performed to remove contaminants of the surface of the targets. The process was kept for 5 min, and then the baffle was opened. The sputter chamber was evacuated to a pressure smaller than 6.0×10^{-4} Pa and the working pressure used was 0.4 Pa with 40.0 sccm of Ar.

The sputtering power of Zn was 46 W and Sb was 26 W, and the sputtering time was set to be 30 min. When Zn and Sb sputtering proceed to 15 min, Bi was start to sputter with the power of 26 W for 0 s, 10 s, 20 s, 30 s, 45 s, 1 min, 2 min, 3 min, respectively. Those samples were analyzed by energy dispersive spectroscopy (EDS), and we selected from these samples with doping contents of 2 at.%, 4 at.%, and 6 at.%. The samples were marked as S2, S3, and S4. Undoped sample was recorded as S1. The details are shown in Table I. All the samples were prepared at the same condition and annealed at 325°C for 1 h under Ar atmosphere with the pressure of 420 Pa after the deposition process finished.

The surface morphology of the thin films were obtained by scanning electron microscopy (SEM) (Zeiss supra 55), and the component analysis proceeded by energy dispersive spectroscopy (EDS). The thin film structure was investigated by x-ray diffraction (XRD) with the prescriptive θ–2θ mode. The room-temperature thermoelectric properties of the thin films were measured by a Seebeck coefficient measurement system (PSM). The thermal conductivity was measured by transient hot-wire theory method at room-temperature. This method uses two metal wires which were kept in a flexible substrate as a heating and testing unit. Then this unit was kept between two same thin film samples and the thermal conductivity can be test and calculated by the thermal conduction principle.[14,16] The thickness of the thin films was obtained by using a Dektak3 ST surface-profile measurement system (Rigaku Ultima4). Carrier concentration was obtained from Hall Effect measurements.

RESULTS AND DISCUSSION

Figure 1 shows the XRD pattern of all the thin films. The results indicate that all the samples have four main diffraction peaks, which match the ZnSb standard peaks. There are only few impurity diffraction peaks of Zn and Bi. This shows that the samples have primary ZnSb phase after the Bi is doped. But compared with the undoped sample, the diffraction peak angle of the doped samples has a little excursion. This phenomenon demonstrates that the tension of the thin film increases after doping with Bi. It can influence the crystal lattice constant and then change the site of the diffraction peak. The measurements show that the samples S2–S4 have a better preferred orientation after the Bi element is added. From the XRD patterns, we can confirm that all the thin films have primary ZnSb phase and the sample has better crystallinity after Bi doping.

The SEM images can be found in Fig. 1. The SEM Images show little change in the surface topography with increasing Bi-doping content. The undoped sample S1 is uniform and the grain size has litter increase after Bi doped. This result confirmed that there is no obvious relationship between the surface topography of thin films after Bi doping.

Carrier concentration was obtained from Hall effect measurements, and the majority charge carriers in all the samples are holes. In order to understand the change in behavior of the resistivity (the reciprocal of electrical conductivity) and the Seebeck coefficient of ZnSb, the carrier

Table I. Parameters of samples

Sample	S1	S2	S3	S4
Zn, Sb sputtering time	30 min	30 min	30 min	30 min
Bi sputtering time	0 s	20 s	1 min	2 min
Bi-doped contents	0 at.%	2 at.%	4 at.%	6 at.%

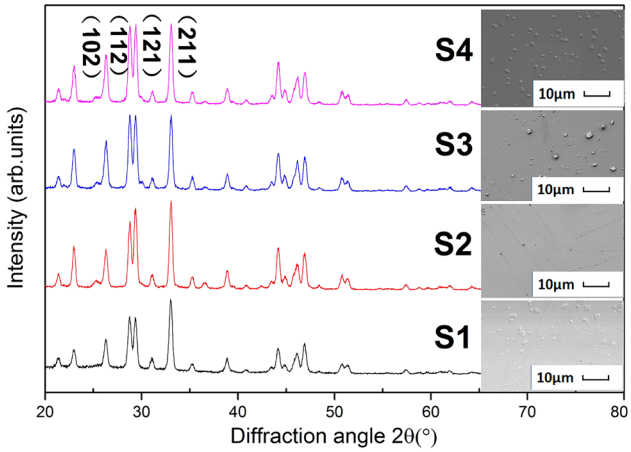

Fig. 1. XRD and SEM patterns of Bi-doped Zn-Sb thin films.

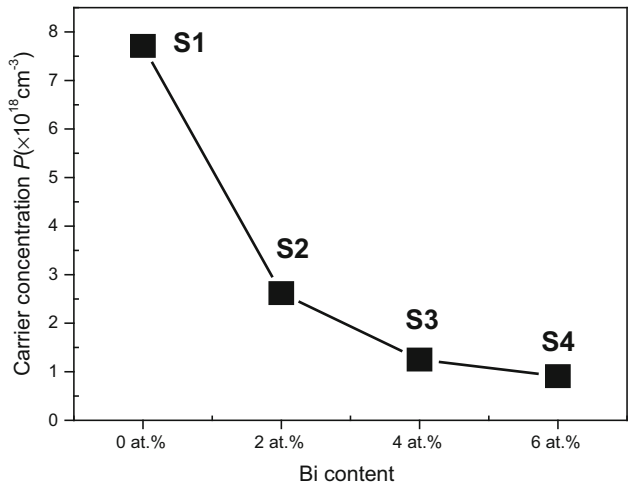

Fig. 2. Variation in the room-temperature carrier concentration p of ZnSb with different Bi contents.

concentration transformation with the different doping contents was determined by the measurements of Hall coefficient. As shown in Fig. 2, the result is related to the specific fabrication conditions, e.g. annealing temperature, leading to different interstitial Zn atoms contained. Furthermore, it can be seen from Fig. 2 that the concentration of ZnSb decreases from 7.71×10^{18} cm^{-3} to 0.91×10^{18} cm^{-3} when the Bi content increases. Therefore, the result demonstrates that these changes in both the resistivity and Seebeck coefficient with doping content are mainly caused by the change of carrier concentration. It is worthwhile to point out that the increase in Seebeck coefficient (S) is due to the light doping with electron donors. It is similar to β-Zn_4Sb_3 predicted and suggested in Ref. 17.

Figure 3a gives the room-temperature Seebeck coefficient of ZnSb with the different doping contents. It can be seen that the Seebeck coefficient of

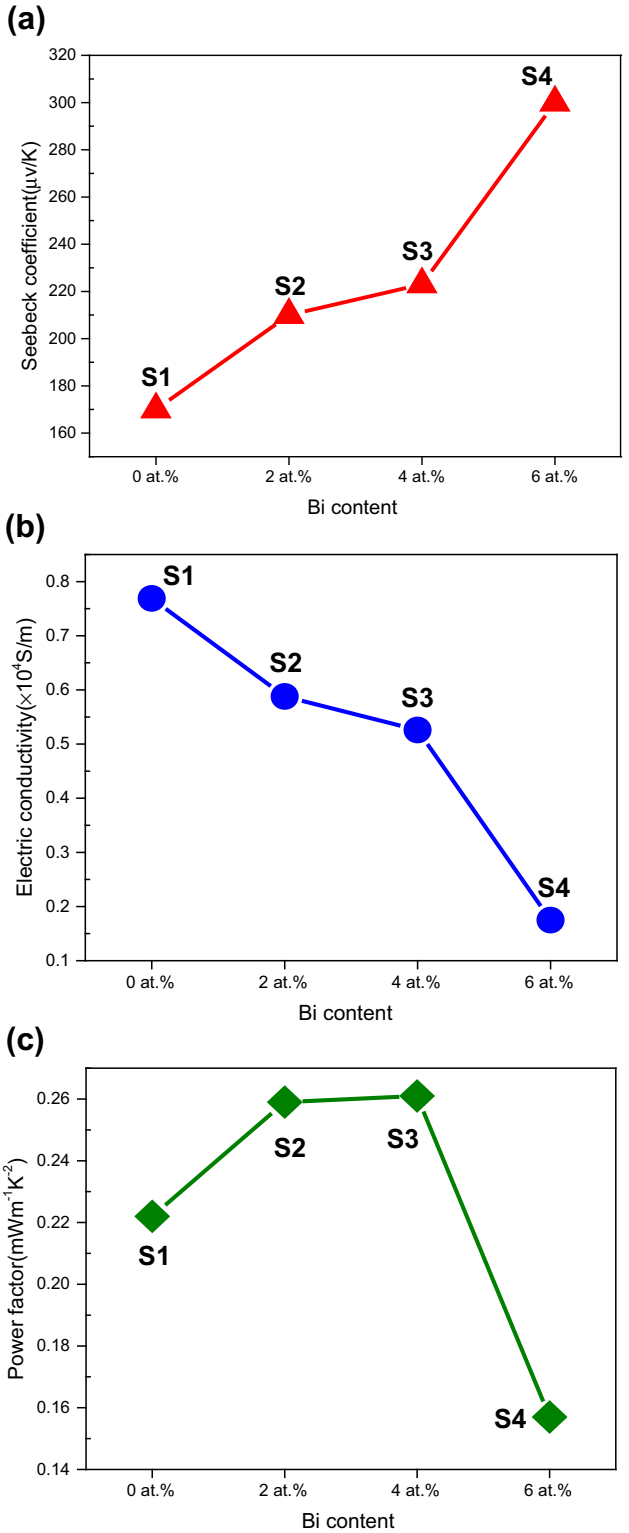

Fig. 3. Variation in the room-temperature Seebeck coefficient (a), room-temperature electrical conductivity (b), and power factor (PF) (c) of ZnSb with different Bi contents.

ZnSb increases remarkably from 170 μVK^{-1} to 300 μVK^{-1} when the Bi content increases from 0 at.% to 6 at.%. Figure 3b shows that the room-

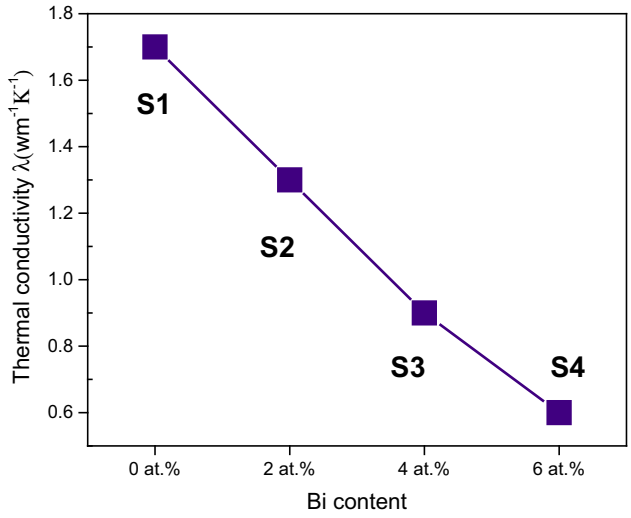

Fig. 4. Variation in the room-temperature thermal conductivity of ZnSb with different Bi contents.

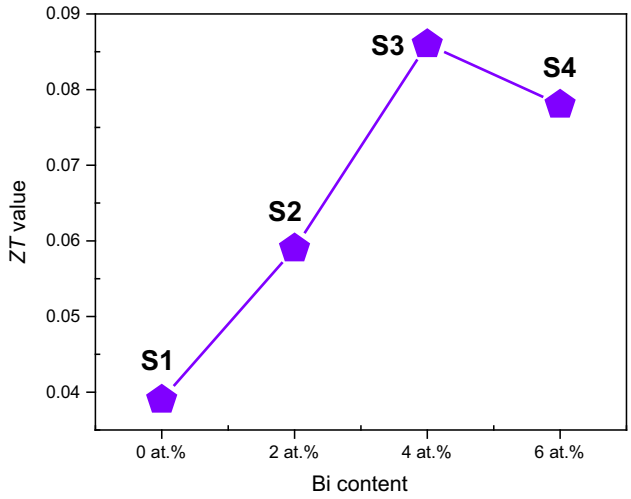

Fig. 5. Variation in the room-temperature ZT value of ZnSb with different Bi contents.

temperature electrical conductivity decreases from $0.769 \times 10^4\ \mathrm{Sm}^{-1}$ to $0.175 \times 10^4\ \mathrm{Sm}^{-1}$ after Bi doping. This is probably arise from the differences in microstructures, such as differences in grain sizes, as well as their distributions or carrier concentrations, including following examination of the samples obtained under different fabrication conditions.

By comparing Fig. 3a with b, the change in Seebeck coefficient of ZnSb with doping content has the opposite behavior to that of the electrical conductivity. This phenomenon strongly suggests that the change in both resistivity (the reciprocal of electrical conductivity) and Seebeck coefficient originate from the same physical mechanism. From Seebeck coefficient (S) and electrical conductivity (σ), we can get the power factor (PF) of ZnSb with different Bi contents, as shown in Fig. 3c. This shows that the values of PF increase firstly and then decrease. This is associated with the sharp decrease in conductivity. The S3 sample has a higher PF than the other samples. The thermoelectric property of S3 is greatly optimized and the PF can reach $0.26 \times 10^{-3}\ \mathrm{Wm}^{-1}\ \mathrm{K}^{-2}$.

Thermal conductivity of the thin films with various Bi contents was measured and is shown in Fig. 4. It can be seen that the thermal conductivity for ZnSb decreases with the increasing Bi content. Bi atoms distribute in the host lattice with different doping contents, which causes stronger phonon scattering and leads to the lower thermal conductivity.

Combined with Figs. 3 and 4, we can finally get the thermoelectric figure of merit, and the result is shown in Fig. 5. Compared with other samples, S3 has a higher ZT and it reaches 0.086, which is almost three times larger than the value of the undoped sample.

CONCLUSION

In this work, we have studied the effects of Bi doping on thermoelectric property of ZnSb thin film. The results indicate that the ZnSb electrical conductivity decreases and Seebeck coefficient increases after Bi doping. As a result, it was found that the sample has a large Seebeck coefficient of 300 μV/K when the Bi content is 6 at.%. Carrier concentration provided further profound understanding into the electrical conductivity and Seebeck coefficient. Also, the power factor of the sample with a Bi doping of 4 at.% reaches an optimal value of 0.26 $\mathrm{mW/mK}^2$ and the ZT reaches 0.086.

ACKNOWLEDGEMENTS

Supported by National Natural Science Foundation of China (No. 11604212), Special Project on the Integration of Industry, Education and Research of Guangdong Province (2012B091000174), Key platform and research projects, Education and Research of Guangdong Province (2015KQNCX139), Basical Research Program of Shenzhen (JCYJ201603071 13206388).

REFERENCES

1. G.J. Snyder and E.S. Toberer, *Nat. Mater.* 7, 105 (2008).
2. L.E. Bell, *Science* 321, 1457 (2008).
3. P. Fan, Z.H. Zheng, Z.K. Cai, T.B. Chen, P.J. Liu, X.M. Cai, D.P. Zhang, G.X. Liang, and J.T. Luo, *Appl. Phys. Lett.* 102, 033904 (2013).
4. P. Fan, Z.H. Zheng, Y.Z. Li, Q.Y. Lin, J.T. Luo, G.X. Liang, X.M. Cai, D.P. Zhang, and F. Ye, *Appl. Phys. Lett.* 106, 073901 (2015).
5. V. Andrei, K. Bethke, and K. Rademann, *Energy Environ. Sci.* 9, 1528–1532 (2016).
6. T.M. Tritt, *Science* 272, 1276 (1996).
7. J.P. Heremans, V. Jovovic, E.S. Toberer, A. Saramat, K. Kurosaki, A. Charoenphakdee, S. Yamanaka, and G.J. Snyder, *Science* 321, 554 (2008).
8. D.W. Song, W.L. Liu, T. Zeng, T. Borca-Tasciuc, G. Chen, J.C. Caylor, and T.D. Sands, *Appl. Phys. Lett.* 77, 3854 (2000).

9. G. Chen, *Semicond. Semimet.* 71, 203 (2001).
10. K. Bethke, V. Andrei, and K. Rademann, *PLoS ONE* 11, 1 (2016).
11. M. Telkes, *J. Appl. Phys.* 18, 1116 (1947).
12. P.J. Shaver and J. Blair, *Phys. Rev.* 141, 649 (1966).
13. A.P. Litvinchuk, J. Nylén, B. Lorenz, A.M. Guloy, and U. Häussermann, *J. Appl. Phys.* 103, 123524 (2008).
14. Z.H. Zheng, P. Fan, J.T. Luo, G.X. Liang, P.J. Liu, and D.P. Zhang, *J. Alloy. Compd.* 668, 8 (2016).
15. L. Pan, X.Y. Qin, and M. Liu, *J. Alloy. Compd.* 489, 228 (2010).
16. Z.H. Zheng, P. Fan, Y. Zhang, J.T. Luo, Y. Huang, and G.X. Liang, *J. Alloy. Compd.* 639, 74 (2015).
17. F. Cargnoni, E. Nishibori, P. Rabiller, L. Bertini, G.J. Snyder, M. Christensen, C. Gatti, and B.B. Iversen, *Chem. Eur. J.* 10, 3861 (2004).